

# 3-D X-ray Structural Microscopy with Submicrometer Resolution

B. C. Larson,<sup>1</sup> W. Yang,<sup>1</sup> G. E. Ice,<sup>1</sup> J. Z. Tischler,<sup>1</sup>  
J. D. Budai,<sup>1</sup> J.-S. Chung,<sup>1</sup> K.-S. Chung,<sup>1</sup> W. Lowe<sup>2</sup>  
<sup>1</sup>Oak Ridge National Laboratory, Oak Ridge, TN, U.S.A.  
<sup>2</sup>Howard University, Washington, DC, U.S.A.

## Introduction

We have developed a new and general technique for performing 3-D x-ray structural microscopy (XSM) with submicrometer resolution in all directions [1]. Differential-aperture (knife-edge) profiling of diffracted scattering from white (or monochromatic) microbeams provides submicrometer depth-resolved diffraction patterns that can be analyzed with previously developed 2-D Laue diffraction techniques [2-4]. Since each volume element (voxel) of a sample illuminated by a polychromatic microbeam generates a full diffraction pattern, complete diffraction information is available from each submicrometer voxel by using differential-aperture x-ray (structural) microscopy (DAXM).

## Methods and Materials

Figure 1 illustrates the profiling process that makes it possible to generate diffraction patterns from submicrometer-volume elements. By collecting charge-coupled device (CCD) diffraction images before and after submicrometer steps of the Pt profiling wire, it is possible (by CCD image subtraction) to determine directly the intensity distribution of the scattering that passed through the differential volume of each step of the wire. The source position along the incident microbeam of the differential intensity can then be obtained by geometrical triangulation by using the position of the wire, the position of the CCD pixel collecting the scattering, and their respective distances from the microbeam. Through computer collation of differential intensities as a function of source position for all reflections collected by the CCD, full diffraction patterns can be reconstructed for individual submicrometer voxels along the microbeam direction.

## Results

Figure 2(a) shows the geometry for micrometer-resolution depth-resolved deviatoric (or shear) strain measurements made for bent silicon on the Michigan-Howard-Lucent Technologies-Bell Labs Collaborative Access Team (MHATT-CAT) insertion device (ID) beamline by using this technique. The direction of the incident beam relative to the surface normal was 45°, as

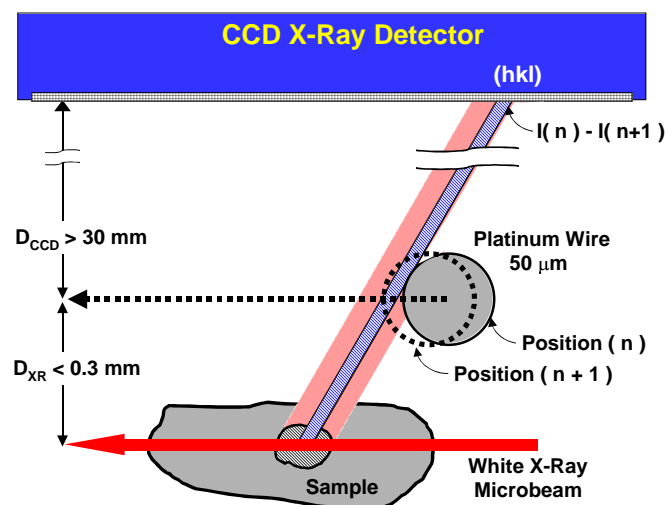


FIG. 1. Schematic view of the differential-aperture depth-triangulation method for determining the source along a polychromatic microbeam of diffracted intensities from Bragg peaks. The difference in intensity in pixels of images collected before and after a submicrometer step of the profiling wire represents the diffracted intensity passing through the step advance distance of the wire. For  $D_{CCD} \gg D_{XR}$  the source of intensity of each pixel can be determined with submicrometer precision by triangulation.

illustrated in the lower left panel of Fig. 2. Diffracted beam profiling measurements were made on both flat and cylindrically bent ( $R = 3.3 \text{ mm}$ ) Si crystal plates about 25- $\mu\text{m}$  thick. Figure 2(b) shows a depth integrated Laue pattern and two reconstructed depth-resolved Laue patterns. Analysis of individual depth-resolved Laue patterns was used to extract (micrometer by micrometer) white-beam diffraction patterns as a function of depth along the penetration direction of the x-ray microbeam.

The deviatoric strain tensor components as a function of depth were obtained by a least-squares fitting analysis of the individual depth-resolved Laue diffraction patterns,

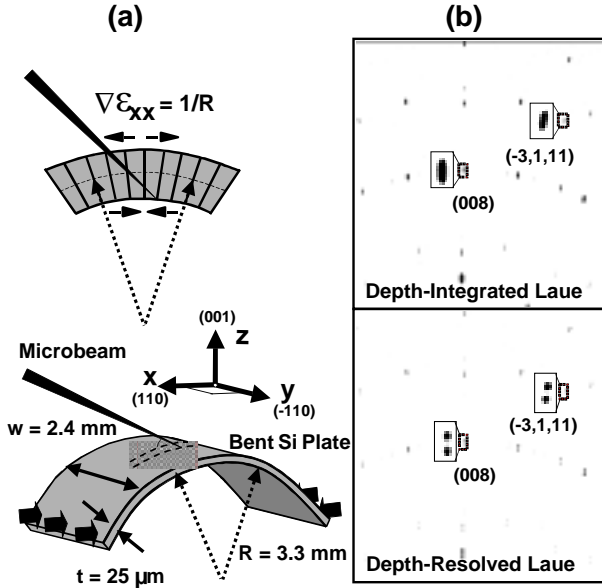


FIG. 2. (a) Schematic view of the strain in a cylindrically bent plate, and a schematic depiction of the x-ray microbeam and the cylindrically bent Si sample. (b) Depth-integrated Laue diffraction pattern from cylindrically bent Si sample (upper), and depth-resolved Laue diffraction patterns from positions near the top surface and near the bottom surface of the sample (lower).

with the unit cell orientation and elastic strain tensor components as fitting parameters [2, 3]. Measurements on the flat (unstrained) Si sample yielded the solid lines in the upper panel of Fig. 3, in which the strain is zero within the  $\sim 10^{-4}$  uncertainty of the measurements. As illustrated schematically in the upper left corner of Fig. 2, the  $\epsilon'_{xx}$  components of the deviatoric strain (i.e., along the bend direction) are large and tensile at the top of the Si arch and large and compressive at the lower surface. The measured deviatoric strain components are shown as the open markers. As expected, the sign of the component (along the surface normal) is opposite to that of  $\epsilon'_{xx}$  as a result of Poisson compression (extension) along the surface normal at the top (bottom) surface.

Since anticlastic bending vanishes for thin plates cylindrically bent to a small radius of curvature, the “full” strain component  $\epsilon_{yy}$  must be “vanishingly” small as well. Therefore, for this special case, the deviatoric strain component  $\epsilon'_{yy}$  provides a direct measure of the negative of the (isotropic) lattice dilatation associated with the bending strain [2]. Moreover, since the full strain is given by the sum of the deviatoric and dilatational strain, the slope of  $(\epsilon'_{xx} - \epsilon'_{yy})$  for the thin plate is expected to be given by  $1/R$ . The lower panel of Fig. 3 indicates that within the

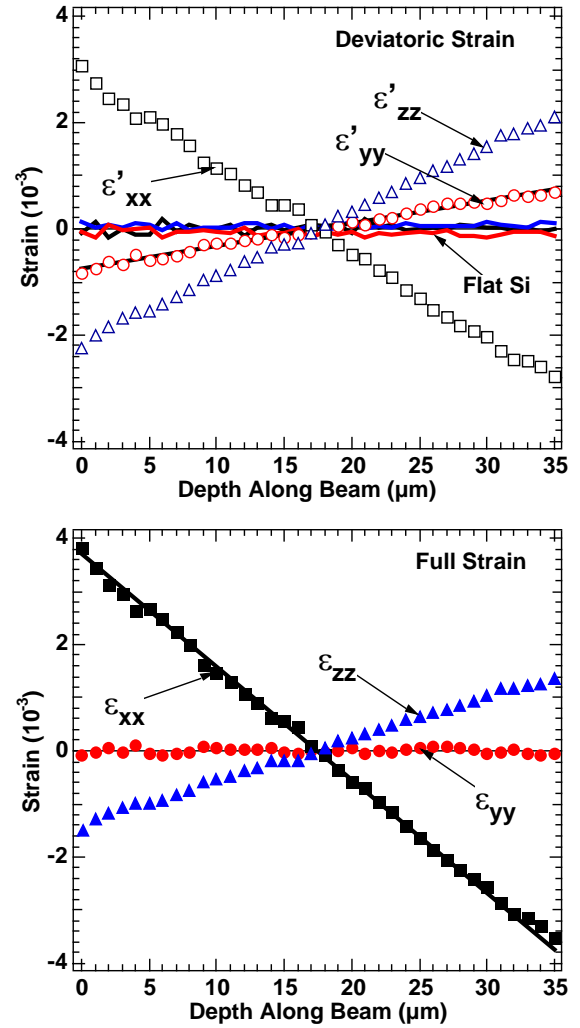


FIG. 3. Depth-resolved deviatoric elastic strain tensor components for flat and cylindrically bent Si plate (upper), and full strain tensor components for cylindrically bent Si plate (lower). Solid line represents the strain gradient expected for a bend radius of  $R = 3.3 \text{ mm}$ .

uncertainties in the measurements, the gradient of  $(\epsilon'_{xx} - \epsilon'_{yy})$  in the  $z$  direction corresponds to the  $R = 3.3\text{-mm}$  radius of curvature measured by direct Laue diffraction measurement of the orientation change along the arch bend direction.

## Discussion

The ability to obtain full diffraction patterns from submicrometer volumes is of fundamental significance for mesoscale materials investigations. It represents a general technique for determining the local crystallographic orientation, phase, morphology, and full stress/strain

tensor for single crystals, polycrystals, deformed materials, composites, functionally graded materials, etc. Nondestructive information of this type will provide a critical link with numerical simulations and multiscale modeling for generating a fundamental understanding of materials microstructure and evolution on mesoscopic length scales of tenths to hundreds of micrometers.

This new capability of using polychromatic microbeams is complementary in technique and spatial resolution to the 10- to 25- $\mu\text{m}$ , 3-D, spatially resolved [5], grain-centroid, grain-average, and, in some cases, real-time capabilities [6-7] developed and demonstrated by the RISØ group by using the European Synchrotron Research Facility (ESRF). X-ray microbeam investigations of materials microstructure and evolution on mesoscopic length scales of tenths to hundreds of micrometers are advancing rapidly. The field is in its infancy, and major advances in instrumentation and techniques can be expected on many fronts. Accordingly, continued detailed microbeam measurements; direct, detailed comparisons between these measurements; and results from computer simulations and multiscale modeling are critically needed to provide the basis for a fundamental understanding of microstructural evolution on the mesoscale.

## Acknowledgments

This research was sponsored by the Division of Materials Sciences, U.S. Department of Energy (DOE), under Contract No. DE-AC05-00OR22725 with UT-Battelle, LLC. Experiments were performed on the MHATT-CAT and University-National Laboratory-Industry (UNI)-CAT beamlines funded by the DOE Office of Science, Office of Basic Energy Sciences (BES). Use of the APS was supported by the DOE BES under Contract No. W-31-109-ENG-38.

## References

- [1] B. C. Larson, W. Yang, G. E. Ice, J. D. Budai, and J. Z. Tischler, *Nature* **415**, 887-890 (2002).
- [2] J.-S. Chung and G. E. Ice, *J. Appl. Phys.* **86**, 5249-5255 (1999).
- [3] N. Tamura, J.-S. Chung, G. E. Ice, B. C. Larson, J. D. Budai, J. Tischler, and M. Yoon, *Mater. Res. Soc. Symp.* **563**, 175-180 (1999).
- [4] G. E. Ice and B. C. Larson, *Adv. Eng. Mat.* **2**, 643-646 (2000).
- [5] H. F. Poulsen, S. F. Nielsen, E. M. Lauridsen, S. Schmidt, R. M. Suter, U. Lienert, L. Margulies, T. Lorentzen, and D. Juul Jensen, *J. Appl. Crystallogr.* **34**, 751-756 (2001).
- [6] L. Margulies, G. Winther, and H. F. Poulsen, *Science* **291**, 2392-2394 (2001).
- [7] E. M. Lauridsen, D. Juul Jensen, H. F. Poulsen, and U. Lienert, *Scripta Mater.* **43**, 561-566 (2000).